

Broadband optical switch based on an achromatic photonic gauge potential in dynamically modulated waveguides

Ian A. D. Williamson and Shanhui Fan*

Department of Electrical Engineering, Stanford University, Stanford, California 94305, USA

(Dated: July 21, 2022)

We demonstrate that a photonic gauge potential, which arises from the phase degree of freedom in dynamic refractive index modulation and hence is achromatic, can be used to achieve a broadband optical switch using the configuration of a photonic Aharonov-Bohm interferometer (ABI). The resulting ABI switch has a far larger bandwidth and lower cross talk than the conventional Mach-Zehnder interferometer (MZI). Using coupled mode theory and full-wave numerical modeling, we compare the response of the two interferometers in the presence of nonidealities. Our results indicate the importance of the photonic gauge potential for broadband optical signal processing.

I. INTRODUCTION

It was recently shown that in photonic structures undergoing dynamic refractive index modulation, the phase degree of freedom in the modulating waveform corresponds to a gauge potential for photons. Such a gauge potential has been used to construct photonic Aharonov-Bohm interferometers [1, 2], optical isolators [3] and circulators [4–6], and to demonstrate non-trivial topological photonic effects [7–10].

An effect of a gauge potential is to induce a phase shift for photons [11–15]. However, unlike the usual phase associated with the propagation of light over a distance, a phase shift due to the gauge potential as induced by dynamic modulation is achromatic. Exploiting this characteristic, in this article we show that the bandwidth of an optical switch constructed from the photonic version of the Aharonov-Bohm interferometer (ABI) [16], which utilizes such a gauge potential, can be far broader compared to the standard Mach-Zehnder interferometer (MZI). Our work highlights the importance of the concept of the photonic gauge potential for optical information processing.

II. BASIC CONCEPT

We first review the MZI in the push-pull configuration shown schematically in Fig. 1a. The MZI consists of two 50:50 waveguide couplers connected by parallel waveguide arms of length L . For an incident optical signal in port one, the transmission to port two and port three are given by

$$T_{21} = \sin\left(\frac{\phi_t - \phi_b}{2}\right) \quad (1)$$

$$T_{31} = \cos\left(\frac{\phi_t - \phi_b}{2}\right), \quad (2)$$

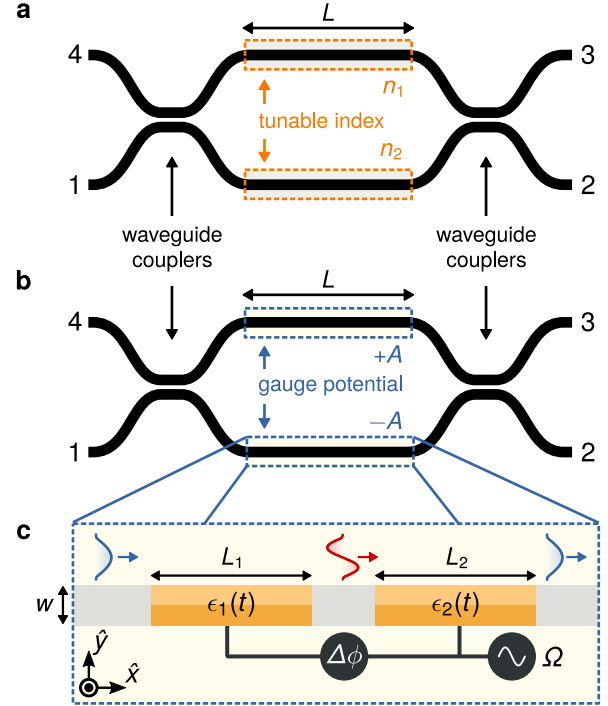


FIG. 1. (a) Mach-Zehnder interferometer (MZI) in a push-pull configuration constructed from 50:50 waveguide couplers connected by parallel interferometer arms with tunable refractive indices $n_{1,2}$. (b) Aharonov-Bohm interferometer (ABI) constructed from 50:50 waveguide couplers connected by parallel interferometer arms with photonic gauge potentials $\pm A$. (c) Implementation of the gauge potential by a sequence of two dynamically modulated waveguides creating photonic transitions.

where the propagation phases in the top and bottom arms are

$$\phi_{t,b} = \frac{2\pi L}{\lambda_0} n_{t,b}. \quad (3)$$

Such an MZI can operate as an ideal switch for incident light at a wavelength λ_0 . In the *on* state, the effective indices of the arms are equal $n_t = n_b = n_0$, and port one transmits completely to port three but not to port two,

* shanhui@stanford.edu

i.e. $T_{21} = 0$ and $T_{31} = 1$. In the *off* state, the effective index of the waveguides are unequal, where $n_t = n_0 + \Delta n$ and $n_b = n_0 - \Delta n$ for $\Delta n = \lambda_0/4L$, and light is instead transmitted from port one to port two but not to port three, i.e. $T_{21} = 1$ and $T_{31} = 0$. However, such a switch is ideal only at a wavelength of λ_0 and in the vicinity of λ_0 , the contrast between the *on* and *off* states degrades because $\phi_t - \phi_b$ is wavelength dependent.

Like the MZI, the ABI consists of the same 50:50 waveguide couplers and two parallel arms with effective index n_0 and length L . Unlike the MZI, the ABI has gauge potentials with opposite signs, $+A$ and $-A$, in its top and bottom arms as shown schematically in Fig. 1c. As a result of these gauge potentials, photons propagating through the two arms experience a phase shift of

$$\phi_{t,b} = \frac{2\pi L}{\lambda_0} n_0 \pm \int A \cdot dl. \quad (4)$$

From Eq. 2, in the *on* state $\int A \cdot dl = 0$ and in the *off* state $\int A \cdot dl = \pi/2$. Like the MZI, the system operates as an ideal switch at λ_0 . However, unlike the MZI, as long as A is independent of wavelength, ideal switching in the ABI is preserved for any wavelength. Thus, the use of a photonic gauge potential can in principal create an optical switch with infinite signal bandwidth.

In practice, an important measure of the performance of a switch is the contrast ratio, defined as the ratio between $|T_{31}|^2$ in the *on* and *off* states. Since in the *on* state $T_{31} \approx 1$, the contrast ratio is dominated by deviation of T_{31} from zero in the *off* state. Such deviation as a function of frequency determines the bandwidth of the switch. In this paper, we will show that in realistic structures, the ABI can have a lower $|T_{31}|^2$ in the off state over a broad bandwidth as compared to the MZI. Hence, the ABI can have a larger switching bandwidth.

The minimization of $|T_{31}|^2$ in the off state over a broad bandwidth is important in various optical systems. A non-zero $|T_{31}|^2$ in the off state results in cross talk which has significant consequences when the interferometer is used as an electrically-reconfigurable routing element [17–19]. In general, the small signals leaked by the switch in the off state generate interference with downstream circuits by limiting the smallest resolvable signal. For example, in sensing and detection systems such as photonic radar [20, 21], small amounts of interference can severely limit detection sensitivities by overwhelming the extremely faint signals which are of interest. In optical communication and information processing systems, the associated reduction in dynamic range from such interference limits the maximum amount of information which can be sent, or processed, per unit time. Thus, the unique spectral response of the ABI can be of significant interest to many real-world optical systems where signals have substantial bandwidths.

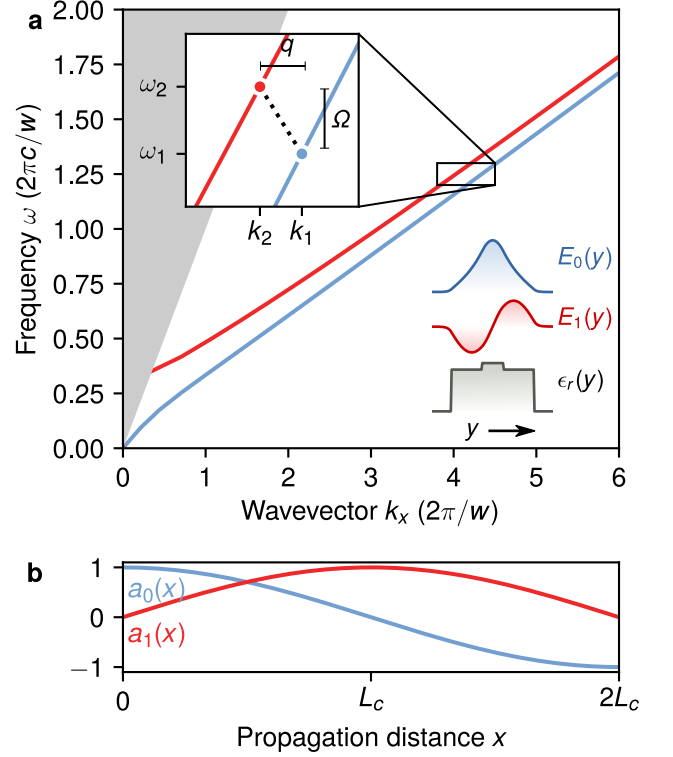


FIG. 2. (a) Dispersion relation and transverse field distributions, $E_{0,1}(y)$ (shown lower right), of the two lowest order waveguide modes for the waveguide with the transverse permittivity profile, $\epsilon_r(y)$ (also shown lower right). The inner core of the waveguide has a width w' and relative permittivity $\epsilon_r = 12.88$ while the outer core has a width w and relative permittivity $\epsilon_r = 12.25$. (b) Spatial evolution of the mode amplitudes, $a_0(x)$ and $a_1(x)$ as they propagate along a section of the modulated waveguide for an input in the zero-order mode, $a_0(x=0) = 1$ and $a_1(x=0) = 0$.

III. PHOTONIC GAUGE POTENTIAL

To construct an ABI, we use photonic transitions in a dynamically modulated waveguide [22–24], as shown in Fig. 1c, to achieve an achromatic gauge potential. The general requirement for such a photonic transition is a waveguide supporting two modes. For example, consider a waveguide with the dispersion relation shown in Fig. 2a, which supports an even and an odd mode. In order to create a gauge potential for photons, the permittivity of two sections of waveguide are modulated with a time-dependence

$$\frac{\epsilon_{1,2}(t)}{\epsilon_0} = \epsilon_r + \Delta\epsilon_r(y) \sin(\Omega t - qx + \phi_{1,2}), \quad (5)$$

where the modulation frequency satisfies

$$\Omega = \omega_1(k_1) - \omega_0(k_0), \quad (6)$$

and the modulation wavevectors satisfies

$$q = k_1 - k_0. \quad (7)$$

We assume weak modulation where $\Delta\epsilon_r/\epsilon_r \ll 1$.

As light propagates along the x -direction in the first modulated waveguide section, as shown in Fig. 1c, energy is parametrically converted from the first-order mode to the second-order mode. Assuming the modulation starts at $x = 0$, for $x > 0$ the field in the waveguide has the form [1, 24]

$$E_0(x, y) = a_0(x)E_0(y)e^{-jk_0x}e^{j\omega_0t} + a_1(x)E_1(y)e^{-jk_1x}e^{j\omega_1t}, \quad (8)$$

where $E_{0,1}(y)$ are the transverse profile of the z -component of the modal electric field (shown in the lower right of Fig. 2a). The modal amplitudes evolve along the direction of propagation as

$$a_0(x) = \cos(Cx) \quad (9)$$

$$a_1(x) = je^{j\phi_1} \sin(Cx), \quad (10)$$

where C , the coupling strength, is

$$C = \frac{\omega^2}{4k_x} \int_0^w \Delta\epsilon_r(y)E_{z0}(y)E_{z1}(y)dy. \quad (11)$$

In order for the two modes to couple, i.e. in order to achieve a non-zero C , the transverse profile of the modulation $\Delta\epsilon_r(y)$ must be nonuniform. In this work we always assume an asymmetric distribution with constant magnitude, $|\Delta\epsilon_r|$ across the waveguide. As shown in Fig. 2b, after propagating for a distance of

$$x = L_c = \pi/2C, \quad (12)$$

an incident wave in the zero-order mode is completely converted to the first-order mode and accumulates a phase of ϕ_1 , as indicated by Eq. 10. Similarly, an incident wave in the first-order mode is completely converted to the zero-order mode over the same distance, but the accumulated phase $-\phi_1$ is opposite in sign.

As shown in Fig. 1c, two modulators with lengths $L_1 = L_2 = L_c$ are placed in each arm of the ABI. As a result, output light after propagating through the two modulated sections has the same frequency and spatial modal profile as the input light, but acquires a phase of

$$\gamma = \pi + \Delta\phi, \quad (13)$$

in addition to the usual propagation phase. Following Ref. 1, $\Delta\phi = \phi_1 - \phi_2$ in Eq. 13 and can be interpreted as a gauge potential for light. Thus, the structure shown in Fig. 1e provides a physical implementation of the ABI interferometer as shown in Fig. 1c.

IV. BANDWIDTH CONSIDERATION

The discussion in the previous section indicates that, in principle, one should be able to achieve an achromatic

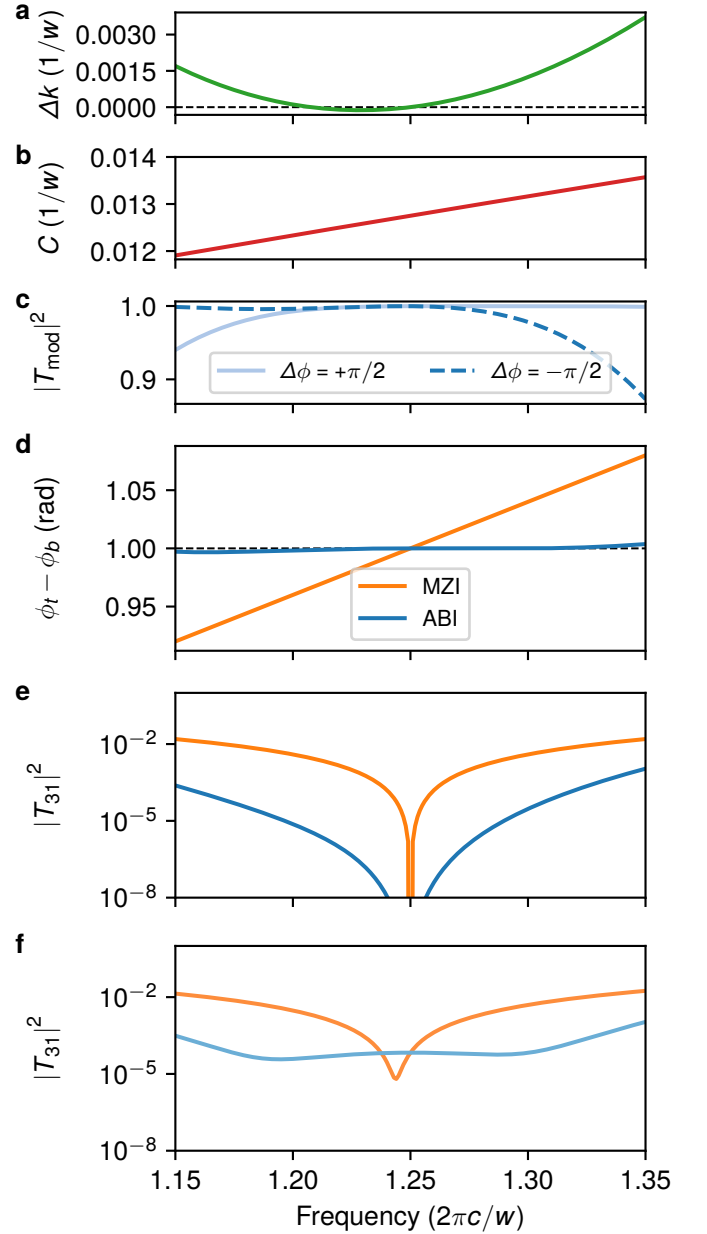


FIG. 3. (a) Phase matching Δk and (b) coupling strength C in units of $1/w$ (inverse waveguide width) as a function of the input frequency for the waveguide shown in Fig. 2a. The input is a zero-order waveguide mode. (c) Transfer function through the two modulators $|T_{\text{mod}}|^2$ for gauge potentials of $\Delta\phi = \pm\pi/2$. (d) Relative phase between bottom and top arms of the ABI (blue), MZI (orange). The targeted phase of $\Delta\phi = \pi$ is indicated by the dashed black line. (e) Transfer function $|T_{31}|^2$ between port 1 and port 3 of the ABI (blue) and MZI (orange). (f) $|T_{31}|^2$ for the ABI (blue) and MZI (orange) with an added frequency-independent phase and amplitude imbalance factor of $0.995e^{-j0.005\pi}$.

gauge potential based on photonic transitions in a waveguide. In practice, to actually achieve such an achromatic gauge potential, one needs to take into account two aspects which may limit the bandwidth: (1) The phase matching condition of Eqs. 6-7, which can be exactly satisfied at one frequency, may not be satisfied over a broad range of frequencies due the group velocity mismatch between the two waveguides, and the group velocity dispersion in each of the waveguides. (2) The coupling constant C given by Eq. 11 may also vary as a function of frequency. Consequently the length of the modulators, designed according to Eq. 12 and hence optimal for one frequency, may not be optimal for other frequencies.

Based on the discussion in Section II, we now focus on the effect of such non idealities on $|T_{31}|^2$ in the off state. We consider the effect of phase matching first. Suppose the phase matching condition of Eq. 6 is satisfied at ω_0 , for a modulation frequency Ω . In the vicinity of the frequency ω_0 , the wavevector mismatch in the photonic transition is given by

$$\Delta k(\omega) = [v_{g0}^{-1}(\omega_0) - v_{g1}^{-1}(\omega_0 + \Omega)] (\omega - \omega_0) + \frac{1}{2} [D_0^{-1}(\omega_0)^{-1} - D_1^{-1}(\omega_0 + \Omega)] (\omega - \omega_0)^2, \quad (14)$$

where $v_{g0,1}$ are the group velocities of the modes, $D_{0,1}$ are the group velocity dispersion parameters of the modes, and ω is the input frequency. Therefore, to reduce the phase mismatch it is important to have a mechanism for controlling the group velocity of the two bands independently.

For the purpose of achieving independent control of the group velocity of the two bands, we consider the geometry shown in the lower right corner of Fig. 2a, which consists of a dielectric region surrounded by air. The dielectric region has an inner core with $\epsilon_r = 12.88$ and width w' and an outer core of slightly lower permittivity $\epsilon_r = 12.25$ and width w . This waveguide design is chosen because the group velocity of the zeroth order mode with even symmetry, which has higher field concentration at the waveguide center, can be tuned independently from that of the first-order mode with odd symmetry by increasing or decreasing w' . We assume a modulation frequency $\Omega = 3.49 \times 10^{-2} (2\pi c/w)$ and a direct transition with $q = 0$, both of which will be used in the subsequent numerical demonstrations. For $w' = 0.26w$, Fig. 3a shows the computed $\Delta k(\omega)$ in the vicinity of $\omega_0 = 1.25 (2\pi c/w)$. $\Delta k(\omega)$ indeed has a parabolic shape, and moreover is relatively small around ω_0 . Thus, with proper design one can indeed achieve a small phase mismatch over a substantial bandwidth.

We now consider the effect of dispersion in the coupling strength, C , as defined in Eq. 11. The dispersion in C arises because the transverse mode profiles vary as a function of frequency. For the system considered here, Fig. 3b indicates that in the frequency range where $\Delta k(\omega)$ is small, C varies by approximately 10%. Thus, the modulator length selected to provide complete conversion at

$\omega_0 = 1.25 (2\pi c/w)$ will not provide complete conversion at higher and lower frequencies.

This dispersion in C affects the transfer function $|T_{\text{mod}}|^2$ through the two modulators as shown in Fig. 3c. Moreover, at $\omega \neq \omega_0$, $|T_{\text{mod}}|^2$ depends on the choice of gauge potential, $\Delta\phi$. The change in $|T_{\text{mod}}|^2$ with $\Delta\phi$ effectively yields an imbalanced insertion loss between the two arms. We emphasize that this effective insertion loss is not dependent on material absorption, but instead results from incomplete conversion between the modes. Any energy in the first order mode after light passes through both modulators is treated as loss because we focus on the interference process in the zeroth order mode. In the full-wave implementation of the ABI we show later, any remaining energy in the first order mode is scattered by waveguide tapering at the ends of the interferometer arms.

Unlike the amplitude response of the modulators, which exhibit dispersion, as shown in Fig. 3c, the phase difference between light passing through the two arms remains very close to π over the entire frequency range considered, as indicated in Fig. 3d. We note that to achieve such a near-achromatic phase shift, the ABI must be operated in a push-pull configuration, where both arms include modulators. This allows any effect of the permittivity modulation on the static waveguide propagation phase to be applied equally to both arms. In contrast, the phase difference between the two arms of the MZI, indicated by the orange line in Fig. 3d, exhibits strong dispersion with a linear frequency dependence from Eq. 3 and a total variation in the phase determined by the relative bandwidth, which is approximately 15%. The relative bandwidth is defined for a frequency range as its width divided by its center frequency.

Fig. 3e compares the transfer function $|T_{31}|^2$ from the lower left port to the top right port in the two interferometers. In the MZI we observe a very narrow dip in the transfer function at $\omega_0 = 1.25 (2\pi c/w)$ with significant degradation in the nulling at lower and higher frequencies. In the MZI, the amplitude responses of the two arms are balanced. At $\omega = \omega_0$, the phase difference between the two arms is exactly π , leading to an exact zero in $|T_{31}|^2$. This degradation in the nulling arises because away from ω_0 , the phase difference between the arms is not π . In the ABI we also observe a dip, but with a much larger bandwidth in the nulling. In the case of the ABI, at the frequency ω_0 , the two arms have a balanced amplitude response, and the phase difference is exactly π , leading to a zero in $|T_{31}|^2$. Away from ω_0 , the phase difference remains at approximately π and the degradation in the nulling instead arises from the different amplitude response of the two arms for two different choices of modulation phases, as shown in Fig. 3c. Across the entire bandwidth considered here, $|T_{31}|$ is always lower in the ABI than in the MZI, even in the presence of the unbalanced signal conversion indicated by Fig. 3c.

In the analysis above, for both the MZI and the ABI, we assume an idealized scenario, where there exists a fre-

quency ω_0 at which the amplitude responses of the two arms are perfectly balanced, and the phase difference is exactly π . In practice, between the two arms there is usually some level of imbalance in the amplitude response, and moreover there may be a background phase difference in addition to the phase differences as considered above.

To illustrate the effect of such nonidealities, Fig. 3f compares the transfer function $|T_{31}|^2$ for the two interferometers with an added factor of $0.995e^{-j0.005\pi}$ in the transmission of the top arm. For both cases, since the two arms are no longer balanced, there is no longer an exact zero in $|T_{31}|^2$. In the case of MZI, the spectrum continues to exhibit a pronounced dip. Due to the linear frequency dependency of the phase difference between the two arms, the additional background phase simply shifts the frequency where the phase difference between the two arms is π . In contrast, in the case of ABI there is no longer a pronounced dip in the spectrum of $|T_{31}|^2$. Because the phase difference between the two arms is largely frequency-independent as shown in Fig. 3d, with an additional background phase the phase difference between the two arms is no longer π within the bandwidth. We also observe that except for the frequencies near the dip in the MZI case, $|T_{31}|^2$ of the ABI is lower over the entire bandwidth of Fig. 3e. Such a flat response in $|T_{31}|^2$ may be potentially advantageous for broadband signal routing because it eliminates the strong dispersion in the cross talk, thus overcoming the tradeoff between maximum signal bandwidth and the amount of interference. In our analysis so far, we have assumed dispersion-free waveguide couplers with an ideal 50:50 splitting ratio. Although, in practical waveguide couplers one should expect dispersion in the splitting ratio, we note that any deviation from 50:50 splitting does not increase T_{31} whenever $\phi_t - \phi_b \equiv \pi$.

V. FULL-WAVE NUMERICAL SIMULATION

We validate the theoretical considerations above using a full-wave frequency domain solution to Maxwell's equations, fully accounting for coupling between the relevant frequency components via the modulation [25, 26]. We consider a two-dimensional computational domain discretized on a Yee lattice surrounded by perfectly matched layer (PML) boundary conditions [27]. For the modulated waveguides in the ABI, we use the same design shown in the lower right of Fig. 2a, but in the waveguide couplers and at the ports we use a narrower waveguide of width $w/10$. This narrower waveguide consists of only a single dielectric material ($\epsilon_r = 12.25$), and allows for a shorter coupling length in the beam splitters due to an increased overlap of the evanescent fields. At the beginning and end of the interferometer arms, the narrower waveguide is tapered to the width w of the modulated sections over a distance of $L_{\text{taper}} = 8w$. Beginning at a distance of $0.75L_{\text{taper}}$ into the tapered waveguide seg-

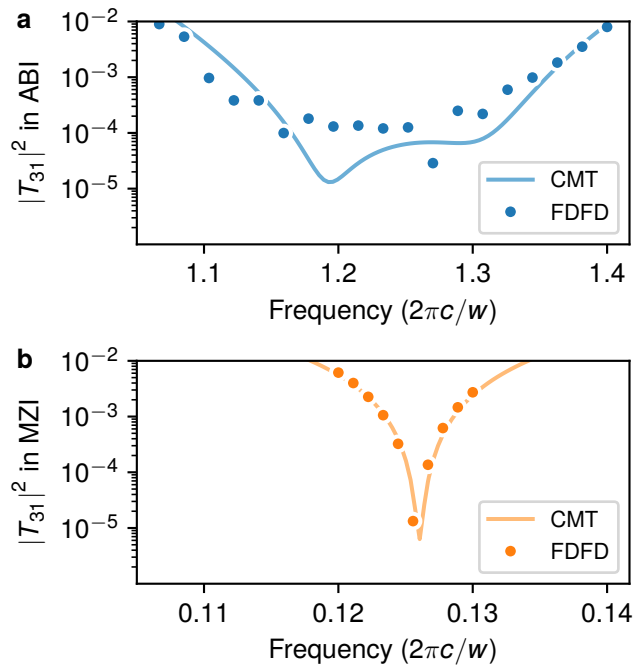


FIG. 4. Transfer function $|T_{31}|^2$ between port 1 and port 3 in the off state for the (a) ABI and (b) MZI computed using the finite difference frequency domain method (FDFD) and coupled mode theory (CMT). The CMT results have an unbalanced phase and amplitude factor of $0.995e^{-j0.005\pi}$ multiplied by the transfer function of the top arm, analogous to the results shown in Fig. 3f.

ment, the permittivity “bump” of width w' is linearly ramped up from 12.25 to 12.88 for the remaining distance of the tapered waveguide, $0.25L_{\text{taper}}$, to match with the modulated waveguide. The permittivity bump is similarly ramped down over a distance of $0.25L_{\text{taper}}$ on the opposite side of the interferometer. Such a continuous linearly increasing permittivity is used for convenience in our numerical simulations and, in practice, other mode-matching techniques can be used between the waveguides. An additional benefit of the waveguide tapering is that the first-order mode, with odd symmetry, is unable to couple into the narrower single-mode waveguide, preventing further interference from residual energy in the first-order mode.

Fig. 4a shows the transfer function $|T_{31}|^2$ in the off state for the ABI, which was computed by numerically integrating the flux over the input and output waveguides. We observe that $|T_{31}|^2$ remains relatively uniform, around a value of approximately 10^{-4} , over a 10% relative bandwidth at the center of the spectrum. The numerical results compare well with the coupled mode theory model as discussed in the previous section, which includes a factor of amplitude and phase imbalance $0.995e^{-j0.005\pi}$ in the transmission of the top arm. The numerical results indicate that the phase shift from the photonic gauge potential is indeed nearly achromatic, but the simulated structure has a small imbalance be-

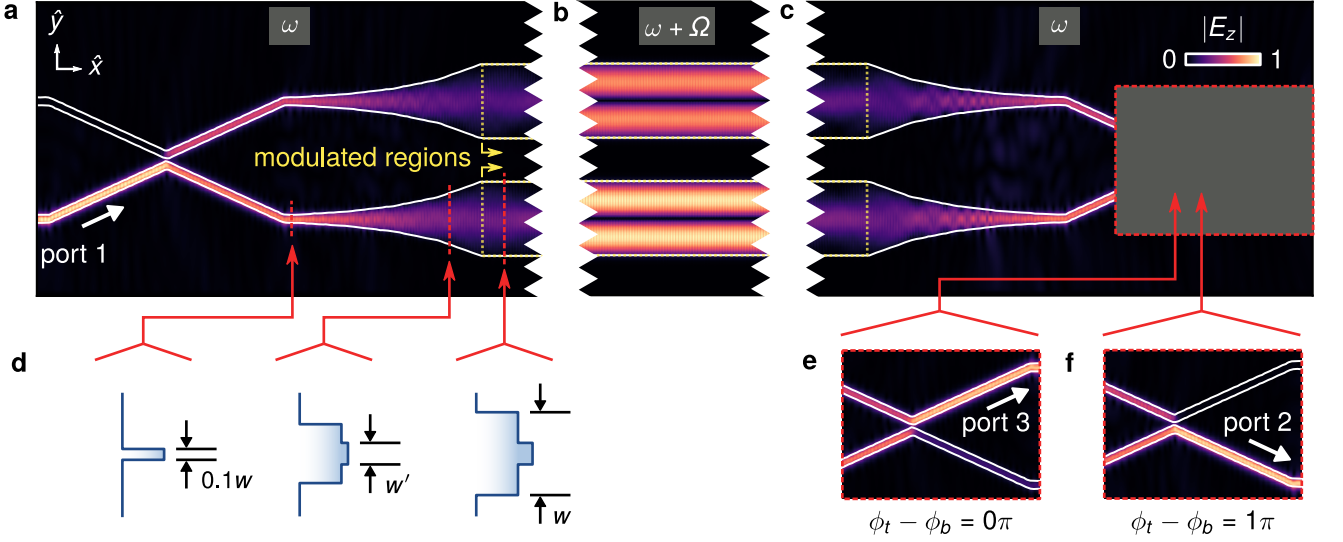


FIG. 5. (a-c) Electric field distribution (magnitude of the z -component) in the ABI for a signal incident from port 1. Panels a and c show the field at the input and output frequency ω while panel b shows the field at the up-converted frequency $\omega + \Omega$ in the middle region of the interferometer. (d) Cross section of waveguide permittivity in the arms and in the couplers. (e,f) Output field magnitude for $\phi_t - \phi_b = 0$ and $\phi_t - \phi_b = \pi$. The horizontal axes of all field distribution plots have been scaled by a factor of $1/3$ with respect to the vertical axes.

tween the two arms, possibly originating from very small reflections off of the waveguide couplers and tapers. Very small reflections from the abrupt boundary of the modulation itself could also contribute to the imbalance observed in the full wave calculation. We note that the waveguide coupler used in the simulation is not 50:50 over the entire spectrum. Such a dispersion in the waveguide coupler, however, does not significantly influence the performance of the switch because the phase difference between the arms is sufficiently close to π over a broad bandwidth.

In contrast, Fig. 4b shows that a full wave simulation of the MZI, with identical waveguide couplers to the ABI, exhibits a response in $|T_{31}|^2$ which varies by several orders of magnitude. This simulation uses the narrower waveguide of width $w/10$ throughout, which results in a lower normalized operating frequency. However, Fig. 4b considers a spectrum with the same relative bandwidth as the ABI calculation in Fig. 4a. Like that of the the ABI, the full-wave simulation of the MZI is consistent with a transfer matrix calculation which includes a phase and amplitude imbalance, largely confirming the theoretical analysis of the previous section. In the case of the MZI, the increased permittivity required to satisfy Eq. 3 likely results in small reflections which act to slightly shift the frequency where $|T_{31}|^2$ reaches its minimum.

Fig. 5a-c show the electric field distribution of the ABI for a signal incident from port 1 at frequency $\omega = 1.25 (2\pi c/w)$. Fig. 5b shows the field at the up-converted frequency $\omega + \Omega$ around the halfway point of the interferometer, while Fig. 5a and Fig. 5c show the field around the waveguide couplers at the input and output

signal frequency ω . The switching of the optical signal at ω between the two output ports is shown in Fig. 5e-f, where the gauge potentials are tuned from $\phi_t - \phi_b = 0$ to $\phi_t - \phi_b = \pi$. For comparison, the field distribution in the MZI at the frequency with the lowest $|T_{31}|^2$ is shown in Fig. 6. These field patterns confirm that the simulated structures indeed function as optical switches.

In the ABI demonstrated in Fig. 5, the modulation is configured with $\Omega = 3.49 \times 10^{-2} (2\pi c/w)$ and $\Delta\epsilon_r/\epsilon_r = 2.45 \times 10^{-3}$, while $L_c = 121.86w$. Taking $w = 2 \mu\text{m}$, the simulation of the ABI operating around $\lambda_0 = 1550 \text{ nm}$ corresponds to a modulation frequency which is two orders of magnitude larger than what is capable in state of the art modulators where $\Omega/2\pi \sim 10\text{-}100 \text{ GHz}$. One approach to using a realistic modulation frequency in the same waveguide design is to instead achieve the gauge potential with an indirect photonic transition where $q \neq 0$. This would make the design similar to the dynamic isolator previously proposed in Ref. 28 where a 1 GHz phonon mode played the role of the modulation. In such an indirect transition, the gauge potential would be retained through a global relative modulation phase shift between the modulated waveguide sections, which would each carry an x -dependent phase from the momentum. An added constraint from using a lower modulation frequency is the need for a smaller modulation index and larger modulator length, such that $\epsilon_r \Omega / \omega \Delta\epsilon_r \gg 1$, to preserve the single-sideband nature of the modulation. Moreover, in a three dimensional waveguide structure additional geometric degrees of freedom, such as a nonuniform out-of-plane waveguide thickness, could be used for dispersion engineering. Three dimen-

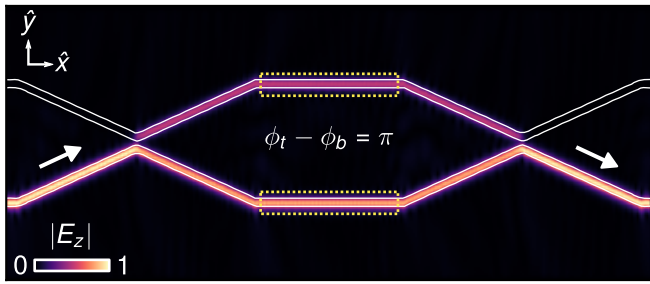


FIG. 6. Electric field distribution (magnitude of the z -component) in the MZI for a signal incident from port 1. The horizontal axis has been scaled by a factor of $1/3$ with respect to the vertical axis.

sional structures also open up the possibility of coupling between modes with different polarizations (e.g. TM-like and TE-like) if electro-optic tensors with the appropriate symmetry are used.

VI. DISCUSSION

In practice, the gauge potential in $\Delta\phi$ would originate from a low frequency phase shifter such as a tunable microwave delay line or resonant phase shifter acting on the modulating waveform. From this perspective, the photonic transition samples such a low frequency dispersive phase shift (at the frequency of the continuous wave modulation), and translates it higher in frequency, by many orders of magnitude, into a broadband optical phase shift. In practice the bandwidth of such a low frequency phase shifter is irrelevant so long as it remains continuously tunable from $0 - 2\pi$ independently of its amplitude response. Unlike the phase shift from a static index shift, the accumulated phase from the gauge po-

tential is not associated with any change in bias amplitude because the peak-to-peak change in the permittivity $|\Delta\epsilon_r|$ remains constant for *all* values of $\Delta\phi$.

It is worth pointing out that Eq. 13 can be interpreted as a form of geometric phase shift which is completely controlled by an electrically tunable modulation phase [29]. This point of view is interesting in contrast with geometric phases which arise in adiabatic nonlinear processes, for example in $\chi^{(2)}$ materials [30]. Nonlinear interactions in these devices can also produce arbitrary geometric phase shifts, but instead require tuning the Fourier coefficients of the quasi-phase matched (QPM) gratings. Such phase shifts are therefore fixed at fabrication while the modulation phase of the photonic gauge potential as discussed here can be dynamically reconfigured at will.

We also note that the dynamics of the ABI and the photonic gauge potential involve only two optical states. In contrast, previous demonstrations of phase shifters based on filtered electro and acousto-optic modulators [31, 32] inherently couple an infinite number of optical states.

VII. CONCLUSION

In conclusion, we have shown that a photonic gauge potential constructed from dynamic modulation can be used to create a broadband switch based on a photonic Aharnov-Bohm interferometer. This work highlights the importance of the photonic ABI and the gauge potential for optical signal processing and computing.

ACKNOWLEDGMENTS

The authors are grateful to Dr. Qian Lin, Dr. Yu Shi, and Dr. Alex Y. Song for many helpful discussions. This work was supported by a U. S. AFOSR MURI Project (Grant N^o FA9550-17-1-0002).

-
- [1] K. Fang, Z. Yu, and S. Fan, Physical Review Letters **108**, 153901 (2012).
 - [2] L. D. Tzuang, K. Fang, P. Nussenzveig, S. Fan, and M. Lipson, Nature Photonics **8**, 701 (2014).
 - [3] H. Lira, Z. Yu, S. Fan, and M. Lipson, Physical Review Letters **109**, 033901 (2012).
 - [4] D. L. Sounas, C. Caloz, and A. Alù, Nature Communications **4**, 2407 (2013).
 - [5] I. A. D. Williamson, S. H. Mousavi, and Z. Wang, ACS Photonics **5**, 3649 (2018).
 - [6] Y. Shi, Q. Lin, M. Minkov, and S. Fan, IEEE Journal of Selected Topics in Quantum Electronics **24**, 1 (2018).
 - [7] K. Fang and S. Fan, Physical Review A **88** (2013), 10.1103/PhysRevA.88.043847.
 - [8] K. Fang and S. Fan, Physical Review Letters **111** (2013), 10.1103/PhysRevLett.111.203901.
 - [9] L. Yuan, Y. Shi, and S. Fan, Optics Letters **41**, 741 (2016).
 - [10] A. Y. Song, Y. Shi, Q. Lin, and S. Fan, arXiv:1806.00544 [physics, physics:quant-ph] (2018), arXiv:1806.00544 [physics, physics:quant-ph].
 - [11] Q. Lin and S. Fan, Physical Review X **4**, 031031 (2014).
 - [12] T. Ozawa, H. M. Price, N. Goldman, O. Zeitler, and I. Carusotto, Physical Review A **93** (2016), 10.1103/PhysRevA.93.043827.
 - [13] Y. Lumer, M. A. Bandres, M. Heinrich, L. Maczewsky, H. Herzig-Sheinfux, A. Szameit, and M. Segev, arXiv:1808.10207 [physics] (2018), arXiv:1808.10207 [physics].
 - [14] F. Liu, T. Xu, S. Wang, Z. H. Hang, and J. Li, arXiv:1803.04594 [physics] (2018), arXiv:1803.04594 [physics].
 - [15] C. Qin, F. Zhou, Y. Peng, D. Sounas, X. Zhu, B. Wang, J. Dong, X. Zhang, A. Alù, and P. Lu, Physical Review Letters **120** (2018), 10.1103/PhysRevLett.120.133901.

- [16] Y. Aharonov and D. Bohm, *Physical Review* **115**, 485 (1959).
- [17] A. Annoni, E. Guglielmi, M. Carminati, G. Ferrari, M. Sampietro, D. A. Miller, A. Melloni, and F. Morichetti, *Light: Science & Applications* **6**, e17110 (2017).
- [18] T. W. Hughes, M. Minkov, Y. Shi, and S. Fan, *Optica* **5**, 864 (2018).
- [19] S. Pai, B. Bartlett, O. Solgaard, and D. A. B. Miller, *arXiv:1808.00458 [physics]* (2018), *arXiv:1808.00458 [physics]*.
- [20] V. J. Urick, J. D. McKinney, and K. J. Williams, *Fundamentals of Microwave Photonics*, Wiley series in microwave and optical engineering (Wiley, Hoboken, New Jersey, 2015).
- [21] P. Ghelfi, F. Laghezza, F. Scotti, G. Serafino, A. Capria, S. Pinna, D. Onori, C. Porzi, M. Scaffardi, A. Malacarne, V. Vercesi, E. Lazzeri, F. Berizzi, and A. Bogoni, *Nature* **507**, 341 (2014).
- [22] J. N. Winn, S. Fan, J. D. Joannopoulos, and E. P. Ippen, *Physical Review B* **59**, 1551 (1999).
- [23] P. Dong, S. F. Preble, J. T. Robinson, S. Manipatruni, and M. Lipson, *Physical Review Letters* **100**, 033904 (2008).
- [24] Z. Yu and S. Fan, *Nature Photonics* **3**, 91 (2009).
- [25] Y. Shi, W. Shin, and S. Fan, *Optica* **3**, 1256 (2016).
- [26] O. Schenk, K. Gärtner, W. Fichtner, and A. Stricker, *Future Gener. Comput. Syst.* **18**, 69 (2001).
- [27] W. Shin and S. Fan, *Journal of Computational Physics* **231**, 3406 (2012).
- [28] C. G. Poulton, R. Pant, A. Byrnes, S. Fan, M. J. Steel, and B. J. Eggleton, *Optics Express* **20**, 21235 (2012).
- [29] L. Ranzani and J. Aumentado, *New Journal of Physics* **16**, 103027 (2014).
- [30] A. Karnieli and A. Arie, *Optics Express* **26**, 4920 (2018).
- [31] P. Ballard, H. Hill, and J. Figoski, *Applied Optics* **17**, 331 (1978).
- [32] M. J. Ehrlich, L. C. Phillips, and J. W. Wagner, *Review of Scientific Instruments* **59**, 2390 (1988).